Applied Catalysis B: Environmental 99 (2010) 279–288

Contents lists available at ScienceDirect

Applied Catalysis B: Environmental

journal homepage: www.elsevier.com/locate/apcatb

$Ce_{0.78}Sn_{0.2}Pt_{0.02}O_{2-\delta}$: A new non-deactivating catalyst for hydrogen production via water–gas shift reaction

Asha Gupta [a], M.S. Hegde [b,*]

[a] Materials Research Centre, Indian Institute of Science, Bangalore 560012, India
[b] Solid State and Structural Chemistry Unit, Indian Institute of Science, Bangalore 560012, India

ARTICLE INFO

Article history:
Received 8 January 2010
Received in revised form 21 June 2010
Accepted 22 June 2010
Available online 1 July 2010

Keywords:
Water–gas shift reaction (WGS)
CO oxidation
Oxygen storage capacity (OSC)
Ceria
Tin

ABSTRACT

We demonstrate the activity of $Ce_{0.78}Sn_{0.2}Pt_{0.02}O_{2-\delta}$, a new catalyst, towards water–gas shift (WGS) reaction. Over 99.5% CO conversion to H_2 is observed at $300 \pm 25\,^{\circ}C$. Based on different characterization techniques we found that the present catalyst is resistant to deactivation due to carbonate formation and sintering of Pt on the surface when subjected to longer duration of reaction conditions. The catalyst does not require any pre-treatment or activation between start-up/shut-down reaction operations. Formation of side products such as methane, methanol, formaldehyde, coke etc. was not observed under the WGS reaction conditions indicating the high selectivity of the catalyst for H_2. Temperature programmed reduction of the catalyst in hydrogen (H_2-TPR) shows reversible reduction of Ce^{4+} to Ce^{3+}, Sn^{4+} to Sn^{2+} and Pt^{4+} to Pt^0 oxidation state with oxygen storage capacity (OSC) of 3500 $\mu mol\,g^{-1}$ at 80 °C. Such high value of OSC indicates the presence of highly activated lattice oxygen. CO oxidation in presence of stoichiometric O_2 shows 100% conversion to CO_2 at room temperature. The catalyst also exhibits 100% selectivity for CO_2 at room temperature towards preferential oxidation (PROX) of residual CO in presence of excess hydrogen in the feed.

1. Introduction

Currently 80% of the world's energy demands are met by fossil fuels. Depletion of fossil fuels and increased concerns to address the problems of pollution related to the use of fossil fuels have led to the concept of 'green chemistry', first formulated by Anastas at EPA, US [1,2]. Green chemistry utilizes renewable raw materials and feedstock, conserves energy and resources and eliminates waste and hazardous materials. Syngas derived from biomass gasification and methane from landfill gas can be converted to hydrogen and consequently provides a potential solution to meet our energy requirements. Hydrogen from biomass is environmental friendly because carbon dioxide released from the process will be recycled into the reformer feed or fixed by photosynthesis, resulting in net zero CO_2 emission [3,4].

Hydrogen, thus, generated can be used in more energy-efficient fuel cells. Fuel cells directly convert the chemical energy of the fuels into electrical energy and are two to three times more efficient than the internal combustion engine. One of the major drawbacks of generating H_2 by reforming natural gas, crude oil and biomass is the co-production of mixture of CO and CO_2, which poison the fuel cell Pt-electrode, and degrades the performance when the CO concentration exceeds 10 ppm [5]. Hence for efficient fuel cell applications, production of pure hydrogen from syngas is important. Therefore WGS reaction, a process of converting CO to H_2, has become a key step for fuel processing. A good WGS catalyst should oxidize CO by H_2O, be cost-effective with high performance, have efficient conversion rates at lower temperature and be robust and stable during stringent start-up/shut-down cycles. Another identified issue of WGS reaction is the formation of methane through the reaction $CO + 3H_2 \rightarrow CH_4 + H_2O$ and/or coke over the catalyst under the conditions of high temperature and low steam content thus consuming 3 mol of hydrogen for every mole of CO consumed in the process decreasing the efficiency of hydrogen production in the WGS reaction [6]. Hence 100% selectivity of hydrogen is yet another criterion for good WGS catalyst from green chemistry point of view.

Recently, ceria based catalysts have been investigated to be an alternative to conventional Cu-ZnO WGS catalyst [7]. Oxides of CuO-ZnO or CuO-ZnO/Al_2O_3 are the commercially used WGS catalysts although their performance is not fully understood and is highly dependent on the synthesis conditions and the nature of the oxide support. To enhance the activity and efficiency of WGS conversion process, Pt-group metal, Au or Cu are usually added in small amounts in ceria-based WGS catalyst [8–14]. CeO_2-based catalyst, in addition to providing oxygen storage property [15] and support for metal dispersion, is non-pyrophoric and does not require complex and lengthy activation steps before usage unlike Cu/ZnO catalysts [9]. WGS reaction involves oxidation of CO and therefore

* Corresponding author. Fax: +91 80 2360 1310.
E-mail address: mshegde@sscu.iisc.ernet.in (M.S. Hegde).

0926-3373/$ – see front matter © 2010 Elsevier B.V. All rights reserved.
doi:10.1016/j.apcatb.2010.06.034

the effectiveness of the catalyst depends greatly upon the ease of reducibility and access to the redox cycles. Therefore, it is desirable to synthesize compounds for WGS reaction with high OSC and high reducibility [16]. The results of Bunluesin et al. [8] demonstrate a strong dependence of WGS reaction rates on the oxygen storage capacity of CeO_2 formulated catalyst. They have shown that a bifunctional redox mechanism between Pt and ceria is responsible for high WGS activity. The present work is focused on developing a new WGS catalyst coupled with high oxygen storage properties to overcome the problems of deactivation of Pt metal supported CeO_2 catalyst reported earlier [17,18]. Recent reports from this laboratory have shown that noble metal ions dispersed ceria, synthesized by solution combustion method, has high rates of CO oxidation compared to noble metal dispersed catalyst [19]. The high rates of CO oxidation are related to ability of the catalyst to use its oxygen storage property. The main course of deactivation is, therefore, attributed to the loss of oxygen storage ability at high temperatures. Hence it is important to formulate catalysts with reversible redox cycling and stability when subjected to higher temperatures. Another reason attributed to deactivation of WGS catalyst is sintering of the noble metal particles at higher temperatures [20]. Although Pt and Au doped CeO_2 has good activity towards WGS reaction, the catalysts get deactivated due to formation of surface carbonate at longer times [17,18,21]. In another report it is mentioned that formation of surface carbonate in La doped ceria is due to basic nature of La^{3+} ion which promotes easy formation of acidic CO_3^{2-} on the surface [22]. Therefore if ceria is doped with ions which are acidic in nature, formation of surface carbonates can be avoided. On the other hand Jacobs et al. rejected the claims that carbonates cause deactivation [23], and reported that surface carbonates are actually formates. In another report, Dorazio et al. [24] claimed that deactivation observed for PtMoRe catalyst supported on zirconia is due to oxidation of the active PtMoRe alloy phase, and heating the catalyst in the reducing gas will regenerate the alloy thereby restoring the activity. Goguet et al. [25] reported that Au supported on $CeZrO_4$ undergo thermal deactivation, and rejected the claims of deactivation due to surface carbonates. In a more recent report by Duarte de Faras et al. [26], deactivation observed for Pt supported in ceria based oxides due to surface carbonate species is mentioned as a secondary or minor factor.

In the present report we have synthesized 2 at.% Pt substituted $Ce_{0.8}Sn_{0.2}O_2$ catalyst by solution combustion method, and found that oxygen storage capacity of the catalyst is reversible even after subjecting the catalyst at high temperature for several cycles. The activity of the catalyst towards WGS reaction at different temperatures and various conditions was determined and compared the results with other catalysts reported in the literature. X-ray photoelectron spectra (XPS) results reveal that Pt is primarily present as Pt^{2+} and Pt^{4+} species due to which sintering of the noble metal ions does not occur. Slow deactivation of the catalyst was not observed even after testing the catalyst for 96 h of start-up/shut-down cycles, and longer duration experiment in presence of excess CO_2 in the feed gas does not show any deactivation due to carbonate formation on the catalyst surface. Sn ion is amphoteric in nature which hinders the formation of surface carbonates unlike La^{3+} ions. The catalyst performance for PROX in presence of excess hydrogen in the feed shows 100% selectivity for CO_2 at room temperature. Combining H_2-TPR and catalytic properties we show that $Ce_{0.78}Sn_{0.2}Pt_{0.02}O_{2-\delta}$ is a promising new catalyst for WGS reaction.

2. Experimental

2 at.% Pt substituted $Ce_{0.8}Sn_{0.2}O_2$ was prepared for the first time by solution combustion method using ceric ammonium nitrate, tin oxalate, tetraamine platinum(II) nitrate and L-tartaric acid (as a fuel). 5.48 g (10 mmol) of $(NH_4)_2Ce(NO_3)_6$ (Loba Chemie, 99%), 0.53 g (2.56 mmol) of SnC_2O_4 (precipitated from $SnCl_2$, Sigma–Aldrich, 99.9%), 100 mg (0.26 mmol) of $Pt(NH_3)_4(NO_3)_2$ (Sigma–Aldrich, 99.9+%) and 4.37 g (29.1 mmol) of L-tartaric acid ($C_4H_6O_6$, Merck, 99%) were weighed, and dissolved in minimum volume of conc. HNO_3 and 20 mL of water in a 300 mL crystallizing dish to form a clear solution. The dish was then kept in a pre-heated furnace at 320 °C. The combustion started after dehydration, and the product was obtained within 60 s. The combustion reaction for preparation of $Ce_{0.78}Sn_{0.2}Pt_{0.02}O_{2-\delta}$ can be written as follows:

$$0.78(NH_4)_2Ce(NO_3)_6 + 0.2Sn(NO_3)_4 + 0.02Pt(NH_3)_4(NO_3)_2 + 2.292C_4H_6O_6 + 0.06O_2\,(\text{air}) \rightarrow Ce_{0.78}Sn_{0.2}Pt_{0.02}O_{1.98} + 9.168CO_2 + 3.58N_2 + 10.116H_2O$$

The products were characterized by powder X-ray diffraction (XRD) (Philips X'Pert Diffractometer fitted with graphite crystal post-monochromator, Cu Kα radiation). Structures were refined by the Rietveld method based on the CeO_2 fluorite structure by means of Fullprof program [27]. For this purpose, XRD data were collected at a scan rate of 0.25° 2θ min^{-1} with 0.01° step size in the 2θ range between 20° and 90°. XPS were recorded on a Thermo Fisher Scientific Multilab 2000 (England) instrument with Al Kα radiation (1486.6 eV). The binding energies reported here is with reference to graphite at 284.5 eV or Ag ($3d_{5/2}$) at 368.2 eV having an accuracy of ±0.1 eV. Oxide samples were ground with 30 wt% graphite powder, made into thin pellet at room temperature. For transmission electron microscopy (TEM) studies, an acetone dispersion of the sample was dropped onto holey carbon coated Cu grids and the images were recorded with FeI Technai 20 instrument at 200 kV.

Oxygen storage/release properties of the catalyst were studied by H_2-TPR carried out in a microreactor (30 cm length and 0.4 cm internal diameter) employing 5.49% H_2/Ar (certified calibration gases mixture obtained from Chemix Speciality Gases and Equipment, Bangalore, India) with 30 sccm flow rate and 10 °C/min linear heating rate up to 450 °C. Volume of hydrogen intake/consumption by the sample was calibrated against CuO standard using an online thermal conducting detector. After every cycle, the catalyst was re-oxidized at 500 °C for 20 min in O_2/Ar and was cooled to 0 °C before carrying out the next TPR cycle. Six such consecutive redox cycles were carried out to check the reversibility of the catalyst.

For WGS catalytic reactions 300 mg catalyst (40/80 mesh) was loaded in the quartz reactor of 4 mm inner diameter and 30 cm length to get a column length of 1.1 cm. Gaseous mixture of 2, 5, 7, 8, 9 and 10 vol% CO were used and the flow rate was adjusted with pure N_2 to keep the total flow at 100 sccm corresponding to dry gas hourly space velocity of 43,000 h^{-1}. Fractional CO conversion vs W/F were plotted at various temperatures and the actual rates were obtained from the slope. The flow rate of water for all WGS reactions was maintained at 2 mL h^{-1}. CO oxidation with H_2O in presence of H_2 was carried out with the feed gas containing 2 and 5 vol% CO, 50 vol% H_2 with N_2 balance to maintain total flow of 100 cm^3 min^{-1}. To check for deactivation of the catalyst, experiments were carried out both in presence and absence of excess CO_2 in the inlet gas stream. 96 h of the start-up/shut-down cycles were performed with inlet gas composition of 5 vol% CO balance with N_2 to maintain a total flow rate of 100 cm^3 min^{-1}. In presence of additional 5 vol% CO_2, deactivation study was carried out for a continuous period of 36 h keeping the conversion of CO at ~30%. XPS of the spent catalysts were recorded to check for any carbonate formation on the surface after testing the catalyst for longer periods of reactions. Catalytic activity over $Ce_{0.78}Sn_{0.2}Pt_{0.02}O_{2-\delta}$ for CO oxidation in presence of O_2 and preferential oxidation of CO by O_2 in presence of excess hydrogen were examined. Gases were analyzed using an online gas chromatograph (ProGC, Mayura Ana-

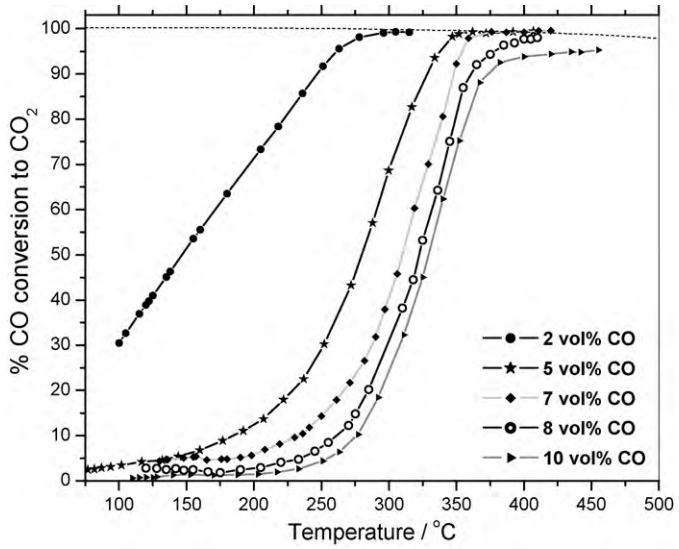

Fig. 1. WGS reaction profiles for different CO concentration over $Ce_{0.78}Sn_{0.2}Pt_{0.02}O_{2-\delta}$ catalyst. Dashed line is the calculated equilibrium conversion under the present feed-gas composition. Reaction conditions: 2, 5, 7, 8, 9 and 10 vol% CO, dry GHSV = 43,000 h^{-1}, 300 mg catalyst and H_2O = 2 mL h^{-1}.

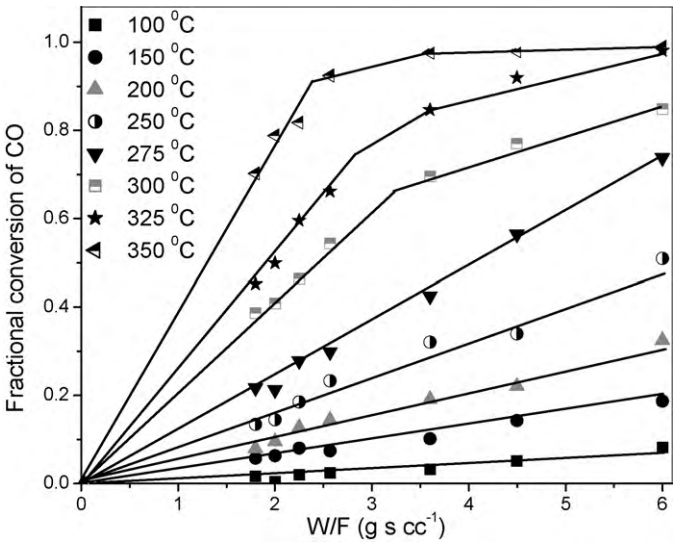

Fig. 2. Fractional CO conversion vs *W*/*F* plot at different temperatures.

lytical Pvt. Ltd., Bangalore) equipped with flame ionization detector and thermal conductivity detector.

3. Results and discussion

3.1. WGS reaction

The fresh catalyst has been tested for WGS reaction in the temperature range between 100 and 500 °C. Fig. 1 shows the effect of temperature on CO conversion in presence of H_2O for different CO concentration. Almost 100% conversion for 2 vol% CO concentration is achieved at 275 °C and more than 99% conversion is achieved at 350 °C for 5 vol% CO concentration while 7 vol% shows ~98% conversion at 360 °C. For 8 vol% CO, 96% conversion is attained at 380 °C and maximum CO conversion of 98% is attained at 410 °C. For still higher concentration of 10 vol% CO, ~93% is converted to CO_2 at 385 °C and maximum conversion of ~95% is achieved at 445 °C. The CO conversion is increasing in the temperature range of 100–475 °C for all CO concentration over the catalyst indicating that CO conversion has not reached equilibrium over the catalyst under the present feed-gas conditions. CO_2 and H_2 were the only products detected in the product stream, and formation of methane (CH_4), methanol (CH_3OH) or formaldehyde (H_2CO) were not observed within our experimental detection limits of ~2 ppm up to 500 °C suggesting high selectivity of the catalyst for hydrogen. It is important to note that with 2 vol% CO concentration almost complete conversion to CO_2 is achieved in spite of the tendency of the equilibrium to shift towards left side in presence of hydrogen produced in the reaction. Further, easy availability of lattice oxygen at low temperature and high CO adsorption probability on Pt ion leads to high CO conversion rates and creation of oxide ion vacancy assists in H_2O dissociation step.

To determine the rate as a function of temperature and activation energy of the WGS reaction over the as-prepared $Ce_{0.78}Sn_{0.2}Pt_{0.02}O_{2-\delta}$, fractional CO conversion vs *W*/*F* were plotted at different temperatures (Fig. 2). The weight, *W*, of the catalyst was kept constant at 300 mg whereas *F*, the flow of CO gas was varied from 3–10 vol% keeping total dry flow rate 100 cm^3 min^{-1}. After each WGS reaction, the next reaction cycle was carried out without any pre-treatment or activation of the catalyst. Slope of linear region of the plot of fractional conversion vs *W*/*F* (the linear region) (see Fig. 2) were used to derive the rates and activation energy for the reaction. Thus, actual rates were obtained for the catalytic activity in the kinetic region. However, by taking suitable amount of catalyst high conversion can be obtained in the kinetic region as shown in Fig. 2. As seen from Fig. 3, the rates of CO conversion over $Ce_{0.78}Sn_{0.2}Pt_{0.02}O_{2-\delta}$ are very high. Arrhenius plot of the reaction rate over the catalyst, shown in the inset of Fig. 3, shows higher activity of $Ce_{0.78}Sn_{0.2}Pt_{0.02}O_{2-\delta}$ catalyst with activation energy, E_a, of 6.7 kcal mol^{-1} compared to literature reported value of 14 kcal mol^{-1} for $Ce_{0.98}Pt_{0.02}O_{2-\delta}$ [22]. A comparison of rate with different Pt containing ceria-based catalysts reported earlier in the literature for WGS activity are given Table 1.

Hydrogen is usually present in large amounts in many practical feed-gas streams. The effect of adding of 50 vol% hydrogen in the feed-gas mixture on the conversion of CO over $Ce_{0.78}Sn_{0.2}Pt_{0.02}O_{2-\delta}$ catalysts was also examined. Fig. 4 shows the effect of presence of H_2 on the equilibrium of the WGS reaction. Presence of hydrogen in the feed-gas shifts the CO to CO_2 conversion towards higher temperature; for 2 vol% CO concentration about 92% conversion is achieved at 330 °C while in absence of hydrogen same concentra-

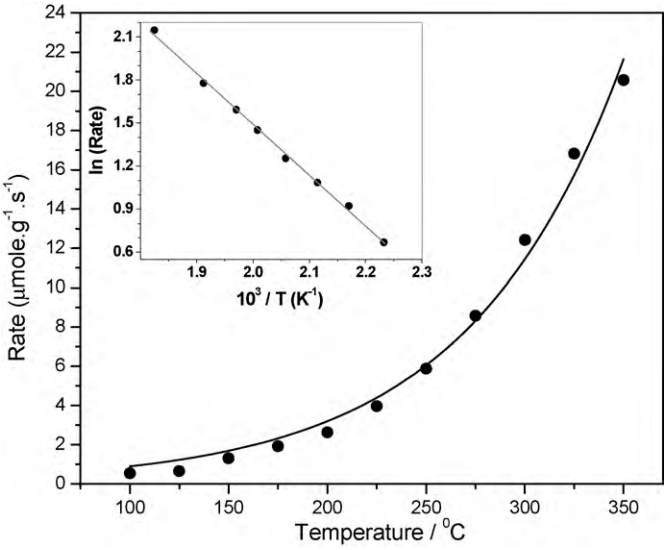

Fig. 3. Differential rates with temperature for the WGS reaction. The inset shows the corresponding Arrhenius plot.

Table 1
Comparison of rates of WGS activity of the present work and results reported in the literature.

Compound	% CO	% H_2O	% H_2	% CO_2	% CH_4	Rate in μmol g^{-1} s^{-1} (temperature)	References
1.18% Pt/CeO_2	6	60	16	1.6	0.4	1.89 (300 °C)	[27]
3.7% Pt 10% La/CeO_2	11	26	26	7		2.0 (350 °C)	[9]
1% Pt/CeO_2	7	22	37	8.5		0.59 (200 °C)	[28]
$Ce_{0.99}Pt_{0.02}O_{2-\delta}$	2	30	50			6.62 (280 °C)	[22]
$Ce_{0.78}Ti_{0.2}Pt_{0.02}O_{2-\delta}$	2	30	50			7.54 (280 °C)	[22]
$Ce_{0.78}Sn_{0.2}Pt_{0.02}O_{2-\delta}$	3.8	25	36			11.1 (300 °C)	Present work

tion of CO is completely converted to CO_2 at 275 °C (from Fig. 1). Equilibrium is achieved at 350 °C and the equilibrium conversion is 93% for this feed-gas composition. For 5 vol% CO concentration, about 85% conversion is achieved at 410 °C in comparison to 350 °C in absence of hydrogen. The CO conversion is always increasing in the temperature range measured up to 450 °C, indicating that equilibrium is not achieved for 5 vol% CO in the present feed-gas composition. Overall decrease of CO conversion is due to establishment of lower equilibrium value in presence high hydrogen (=50 vol%) concentration in the feed gas. Even in presence of large hydrogen in the feed stream CH_4 formation was not detected.

The catalyst was tested for gradual deactivation under the WGS reaction conditions. The catalyst reactor bed which was used initially for determination of activation energy of WGS reaction by varying CO concentration in the feed gas (Fig. 1) was further subjected to start-up/shut-down cycles for total period of 96 h with feed-gas composition of 5 vol% $CO/N_2 + H_2O$ flow. During start-up, the catalyst bed was linearly heated starting from 110 to 350 °C to achieve the steady state conversion for 3 h, followed by cooling of the catalyst to room temperature leading to condensation of water over the catalyst. The catalyst was kept at room temperature for 6 h under full stream dry gas flowing condition and only the temperature was varied and water flow adjusted during start-up cycles to check for any deactivation occurring due to surface carbonate formation. At 350 °C, during the start-up cycles, the steady-state CO conversion of >99%, as observed initially, was achieved and no drop in activity was observed even after 96 h. The catalyst was not subjected to any activation or pre-treatment between cycles (Fig. 5). This clearly indicates that the catalyst is highly active under continuous redox cycling temperatures and does not require any activation unlike conventional commercial CuO-ZnO catalyst. WGS reaction activity of the ionic Pt in $Ce_{0.78}Sn_{0.2}Pt_{0.02}O_{2-\delta}$ is preserved and does not show any deactivation within 96 h of continuous start-up/shut-down cycles. This indicates that $Ce_{0.78}Sn_{0.2}Pt_{0.02}O_{2-\delta}$ catalyst is resistant to deactivation under the present feed-gas condition and operating temperatures.

Deactivation study for WGS activity of the catalyst was also examined in presence of excess CO_2 with an inlet gas composition of 5% CO, 5% CO_2 with N_2 balance keeping dry gas flow rate of 100 cm^3 min^{-1} and water at 2 mL h^{-1}. In presence of CO_2 the equilibrium shifts towards the higher temperature, and 96% CO conversion is achieved at 440 °C (see Fig. 6). After attaining the maximum conversion, the temperature of the reaction was brought down to 250 °C (at which 30% CO conversion is achieved) and was maintained at that temperature for a period of 36 h. The outlet gas was analyzed after every 2–3 h to check for any slow deactivation. No decrease in the percent conversion was observed over the period of 36 h (see Fig. 6), and the sample was further analyzed with XPS to check for carbonate formation.

In an industrial reformer, the outlet gas has a mixture of CO, CO_2, H_2 and several other impurities in smaller percentages. Therefore, it is necessary to test the performance of the catalyst in presence of excess CO_2 and H_2. CO_2 concentration is kept small because it plays a much smaller inhibition role than H_2 [29], and it accumulates during high conversion experiments observed for the present catalyst. Due to presence of both the products H_2 and CO_2 in the feed-gas stream the equilibrium is shifted towards the reactants side due to reversibility of WGS reaction. With 10% H_2 and 5% CO_2 in the feed gas, equilibrium conversion is achieved for two different concentrations of CO (see Fig. 7). For 2% CO concentration equilibrium is attained at 530 °C with 96% CO converted to CO_2, and for 5% CO equilibrium temperature is 535 °C with 98% con-

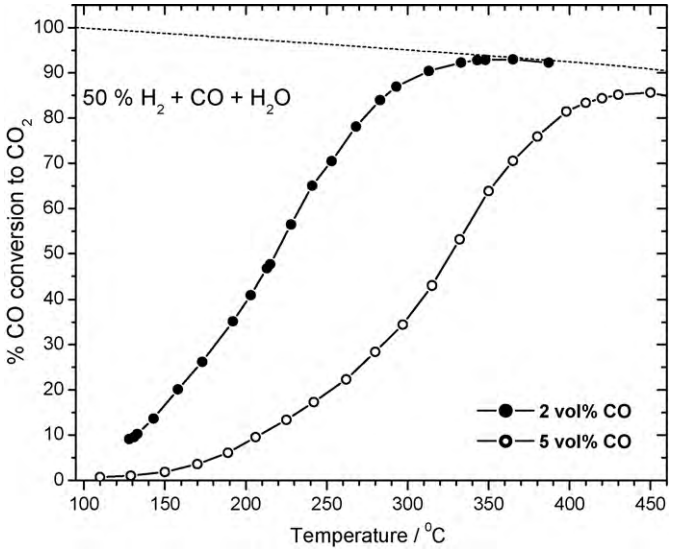

Fig. 4. Effect of H_2 on CO conversion of WGS reaction over the catalyst. Dashed line is the calculated equilibrium conversion under the present feed-gas composition. Reaction conditions: CO = 2 and 5%, H_2 = 50%, dry GHSV = 43,000 h^{-1}, 300 mg catalyst and H_2O = 2 mL h^{-1}.

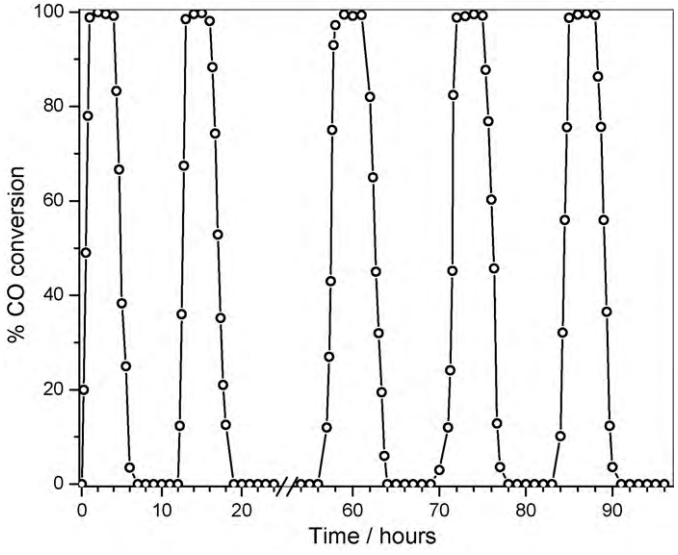

Fig. 5. CO conversion vs time during start-up/shut-down cycles of WGS reaction over $Ce_{0.78}Sn_{0.2}Pt_{0.02}O_{2-\delta}$ catalyst.

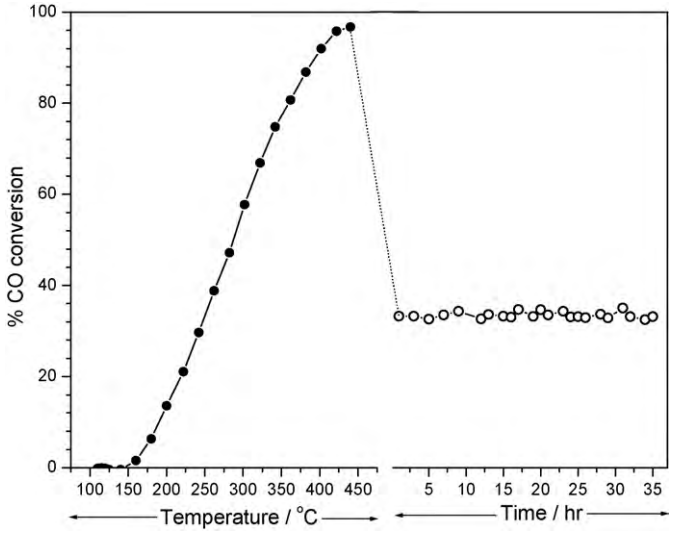

Fig. 6. CO conversion vs temeparture and time in presence CO_2 in the feed gas. Reaction conditions: CO = 5%, CO_2 = 5%, H_2O = 2 mL h^{-1}, dry GHSV = 43,000 h^{-1}, 300 mg catalyst.

version. With the increase of H_2 concentration from 10 to 20% in the feed gas keeping the concentration of CO and CO_2 at 2 and 5% respectively, we observe CO conversion is always increasing for temperature up to 580 °C. Therefore when H_2 concentration is increased in the feed gas the equilibrium conversion could not be attained for $Ce_{0.78}Sn_{0.2}Pt_{0.02}O_{2-\delta}$ catalyst. Here again formation of any product other than CO_2 and H_2 was not detected. Detailed kinetic study is needed to obtain the rates under different feed-gas conditions.

3.2. XRD and TEM

XRD pattern of the as-prepared $Ce_{1-x}Sn_xO_2$, spent catalyst (after 96 h of WGS reaction) and the spent catalyst re-oxidized in air at 400 °C are presented in Fig. 8. Rietveld refinement of the powder XRD pattern was carried out by simultaneously varying 18 parameters that include the overall scale factor, background parameters, unit cell, half width, shape, and isotropic thermal parameters along

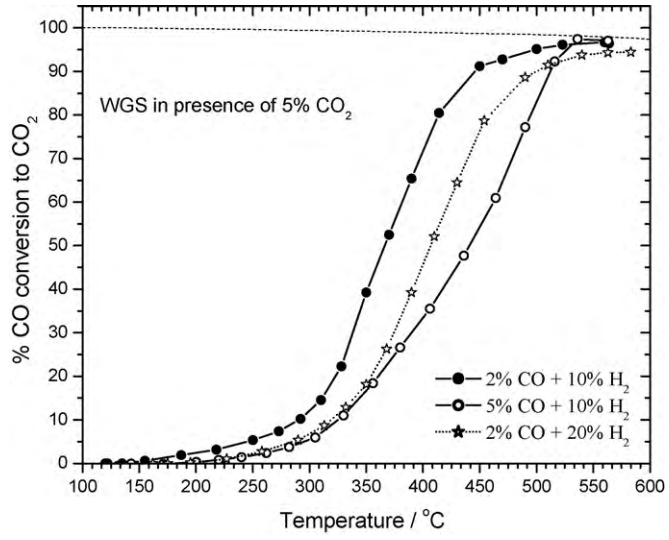

Fig. 7. WGS activity over $Ce_{0.78}Sn_{0.2}Pt_{0.02}O_{2-\delta}$ catalyst in presence of H_2 and CO_2 in the feed gas. Reaction conditions: CO = 2 and 5%, CO_2 = 5%, H_2 = 10 and 20%, H_2O = 2 mL h^{-1}, dry GHSV = 43,000 h^{-1}, 300 mg catalyst.

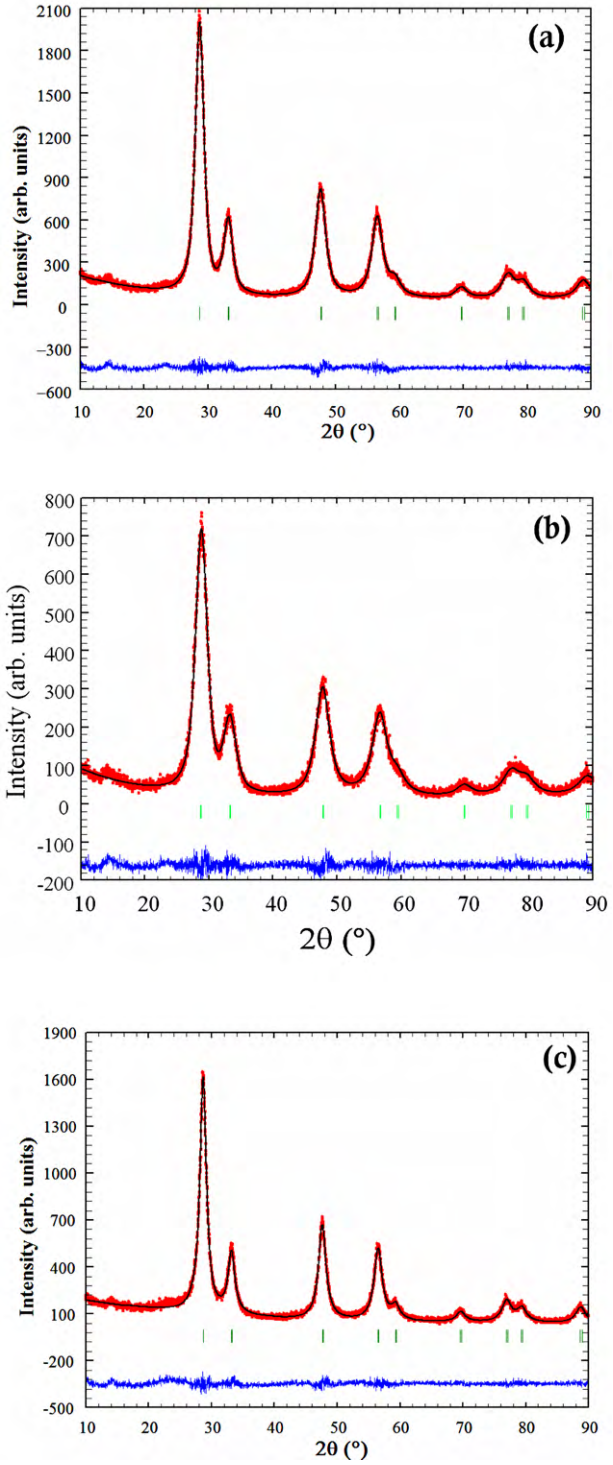

Fig. 8. XRD patterns of $Ce_{0.78}Sn_{0.2}Pt_{0.02}O_{2-\delta}$: (a) as-prepared and (b) spent catalyst after 96 h start-up/shut-down cycles of WGS reaction, (c) same spent catalyst as in (b) heated in air at 400 °C.

with the oxygen occupancy; Sn^{4+} and Pt^{2+} ions were taken in Ce^{4+} sites. The goodness of the profile refinements were determined from the low *R* values, given in Table 2. The typical observed XRD patterns along with the calculated patterns for as-prepared and spent catalyst are shown in Fig. 8. The XRD patterns are identical and could be indexed to the standard CeO_2 with fluorite structure (JCPDS no. 340394). Diffraction lines due tin-oxide was not observed both in as-prepared and spent catalyst. Lattice parame-

Table 2
Rietveld refined lattice parameters of as-prepared and re-oxidized after WGS reaction samples of $Ce_{0.78}Sn_{0.2}Pt_{0.02}O_{1.98}$.

Catalyst	Lattice parameter, a (Å)	R_{Bragg}	R_f	χ^2
CeO_2 (JCPDS No. 340394)	5.411			
$Ce_{0.8}Sn_{0.2}O_{2-\delta}$	5.396 [32]			
$Ce_{0.78}Sn_{0.2}Pt_{0.02}O_{2-\delta}$ as-prepared	5.399	0.98	0.72	1.02
$Ce_{0.78}Sn_{0.2}Pt_{0.02}O_{2-\delta}$ after WGS reaction	5.389	1.05	1.01	0.95
$Ce_{0.78}Sn_{0.2}Pt_{0.02}O_{2-\delta}$ re-oxidized at 400 °C in air after WGS reaction	5.398	1.31	0.69	1.14

ter of the spent catalyst after WGS reaction catalyst is somewhat smaller than that of as-prepared compound (see Table 2). On re-oxidation the resultant lattice parameter is same as that of as-prepared compound.

TEM image of as-prepared $Ce_{0.78}Sn_{0.2}Pt_{0.02}O_{2-\delta}$ are shown in Fig. 9. The bright-field image of $Ce_{0.78}Sn_{0.2}Pt_{0.02}O_{2-\delta}$ is given in panel (a) and the crystallite sizes are in the range of 4–8 nm. Isolated Pt-metal particles were not observed in the bright field image. The inset of Fig. 9a shows the selected area diffraction pattern which is indexed to fluorite structure. Diffraction pattern does not show the presence of additional ring between (2 0 0) and (2 2 0) rings indicating the absence of Pt (1 1 1) metal particles within the detection limits. High-resolution TEM (HRTEM) image, in Fig. 9b, shows 3.1 Å lattice fringes corresponding to $d_{1\,1\,1}$ of $Ce_{0.78}Sn_{0.2}Pt_{0.02}O_{2-\delta}$. Well defined lattice fringes indicate that the particles are crystalline in nature and amorphous phase is not present. Combined XRD and HRTEM results show that CeO_2 and SnO_2 form a complete solid solution in cubic fluorite structure. HRTEM and selected area diffraction pattern of the spent $Ce_{0.78}Sn_{0.2}Pt_{0.02}O_{2-\delta}$ catalyst after WGS reaction are given in Fig. 9c. Separation of phases of SnO_2 and Pt-metal particles were not observed. Again XRD and TEM image of the spent catalyst suggest that the fluorite structure of the catalyst is retained after longer duration catalytic reactions. This implies that the catalyst is stable subjected to WGS reaction condition for a period of 96 h.

3.3. H_2-TPR

Temperature-programmed hydrogen reduction techniques have been extensively used in the literature to characterize the surface and bulk oxygen reducibility of the doped ceria. Yao and Yao reported that reduction peaks of the surface capping oxygen and the bulk oxygen of CeO_2 occurs at 500 and 800 °C, respectively [30]. Substitution of 2 at.% Pt ion in CeO_2 is known to shift the reduction peaks to temperatures as low as −40 °C with H_2/Pt ratio ∼2–3 [31]. Fig. 10 displays the H_2-TPR profiles of $Ce_{0.78}Sn_{0.2}Pt_{0.02}O_{2-\delta}$ catalyst for six cycles and peak reduction temperature for all cycles is at 80 °C. The area under the peak up to 250 °C was used to estimate the oxygen storage capacity (OSC) of the catalyst. OSC of pure CeO_2 and $Ce_{0.8}Sn_{0.2}O_{2-\delta}$ are reported to be 350 and 1650 μmol g^{-1} [32]; on 2 at.% Pt substitution in $Ce_{0.8}Sn_{0.2}O_{2-\delta}$ OSC increases by more than twice of $Ce_{0.8}Sn_{0.2}O_2$ with value as high as 3500 μmol g^{-1}. H_2/Pt ratio estimated for all six cycles is around 28–30, indicating that the H_2 reduction cycles are reversible. Ideally H_2/Pt ratio should be 1 for Pt-metal, whereas ratio H_2/Pt > 1 in the present ionic catalyst indicates the occurrence of simultaneous reduction Pt^{4+}, Sn^{4+} and Ce^{4+} ions. Also substitution of Pt ion in $Ce_{0.8}Sn_{0.2}O_2$ decreases the peak reduction temperature of $Ce_{0.8}Sn_{0.2}O_2$ from 300 to 80 °C.

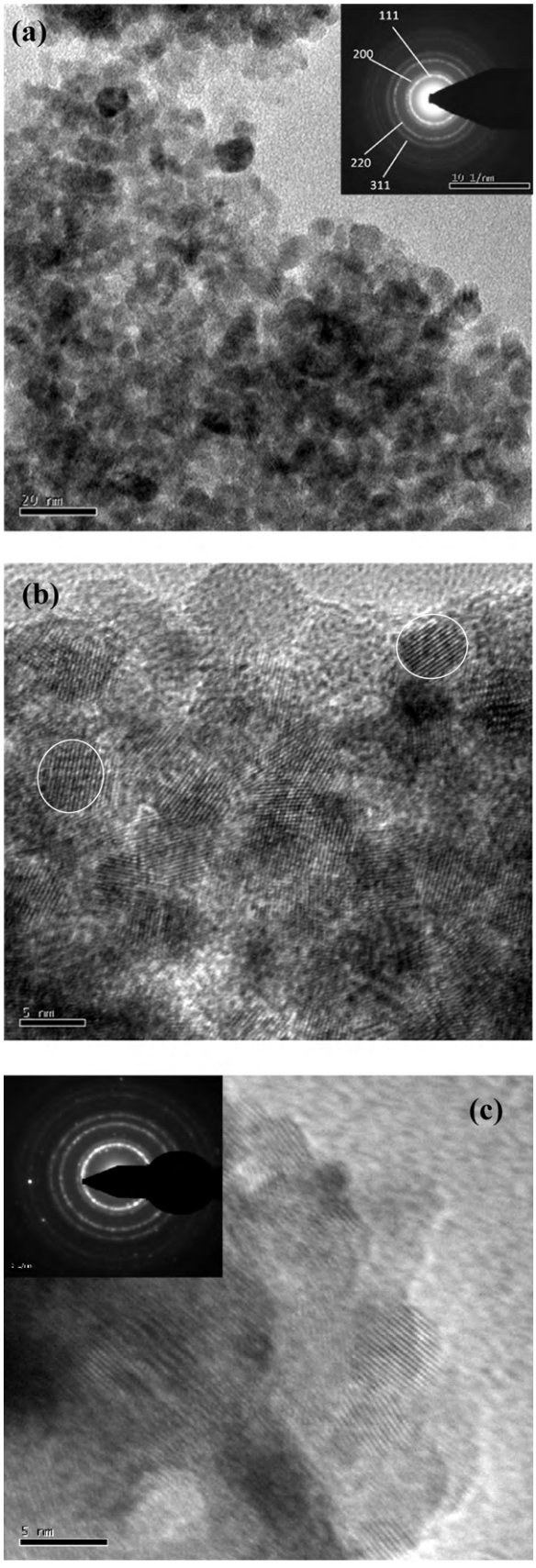

Fig. 9. (a) Bright field image and (b) HRTEM of as-prepared $Ce_{0.78}Sn_{0.2}Pt_{0.02}O_{2-\delta}$ catalyst. (c) HRTEM of the spent catalyst after 96 h WGS reaction. The inset shows the electron diffraction pattern of the respective samples.

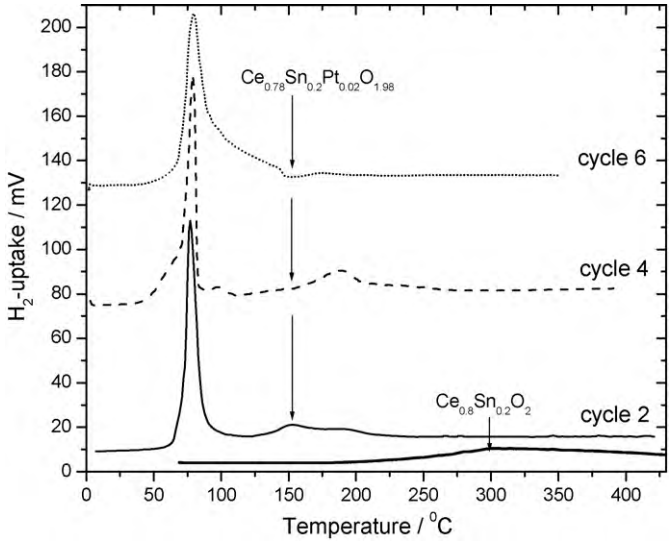

Fig. 10. H_2-TPR measurement of the as-prepared $Ce_{0.78}Sn_{0.2}Pt_{0.02}O_{2-\delta}$ catalyst. H_2-TPR of $Ce_{0.8}Sn_{0.2}O_2$ is given for comparison.

$Ce_{0.78}Sn_{0.2}Pt_{0.02}O_{2-\delta}$ exhibits high reversibility towards hydrogen reduction and attainment of same OSC after every cycle indicate complete recovery of the structure after each reduction-oxidation cycle.

3.4. XPS

Due to condensation of water over the catalyst after WGS reaction, it was difficult to prepare the sample for XPS study. Heating the catalyst under nitrogen flow will lead to oxidation of $Ce_{0.78}Sn_{0.2}Pt_{0.02}O_{2-\delta}$ catalyst due to presence of condensed water. Hence to check the redox states by XPS, the spent catalyst was heated at 150 °C under CO/N_2 flow leading to its reduction. A part of the spent reduced catalyst was re-oxidized in air at 550 °C for 3 h. XPS of as-prepared, reduced and re-oxidized catalyst were recorded.

XPS of Ce (3d) core level, given in Fig. 11a, shows that Ce is mostly in +4 oxidation state with binding energy peaks at 883 and 901 eV corresponding to $3d_{5/2}$ and $3d_{3/2}$ core levels along with the

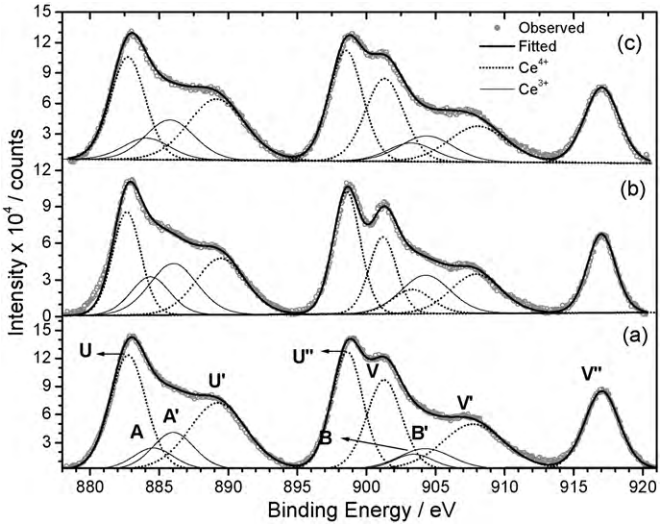

Fig. 11. XPS of Ce(3d) core level of (a) as-prepared catalyst, (b) reduced catalyst after start-up/shut-down cycles, and (c) after re-oxidation of the reduced catalyst in air at 550 °C.

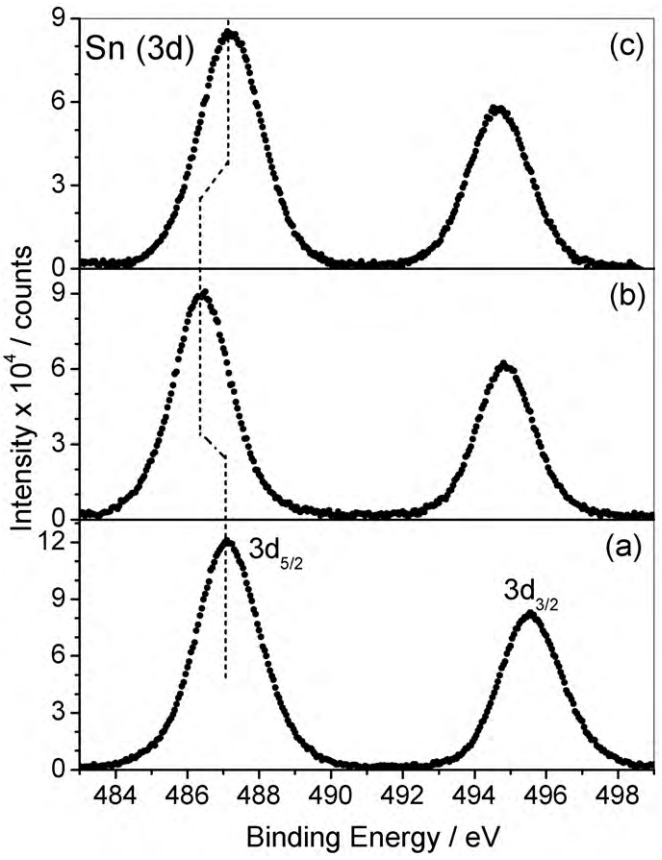

Fig. 12. Sn(3d) core level XPS of (a) as-prepared catalyst, (b) reduced catalyst after start-up/shut-down cycles, and (c) after re-oxidation of the reduced catalyst in air at 550 °C.

characteristic satellite peaks due to Ce^{4+} state as in CeO_2 [33]. A small percentage of Ce is in +3 oxidation state. Resultant deconvolution of the spectra shows that 89% of Ce is present in +4 oxidation state and 11% in +3 oxidation state. The XPS of the reduced sample after 96 h of start-up/shut-down cycles show an increase in Ce^{3+} oxidation state relative to as-prepared catalyst with 30% Ce in +3 oxidation state (Fig. 11b). Re-oxidation of the reduced catalyst produces XPS similar to that of the as-prepared catalyst with Ce^{4+} to Ce^{3+} ratio same as that of as-prepared catalyst (Fig. 11c).

Core level Sn ($3d_{5/2,\ 3/2}$) spectra of as-prepared catalyst have binding energy peaks at 487 and 495.5 eV which corresponds to Sn^{4+} state (Fig. 12a) [34]. XPS of the reduced catalyst has Sn (3d) peaks shifted towards lower binding energy at 486.4 and 494.8 eV which is due to +2 oxidation state of Sn (Fig. 12b) [34]. Taking into consideration the full width at half maxima, it was found that Sn is present completely in +4 oxidation state in the as-prepared sample and is completely reduced to +2 state after WGS reaction. Sn ($3d_{5/2}$) binding energy peak shifts to 487 eV upon re-oxidation indicating complete oxidation of Sn^{2+} to Sn^{4+} (Fig. 12c). Sn^{4+} reduces up to Sn^{2+} state and further reduction to Sn^0 state was not observed under the mentioned reaction conditions (i.e. CO/N_2 reduction condition as mentioned above).

Binding energy of Pt ($4f_{7/2,\ 5/2}$) in as-prepared $Ce_{0.78}Sn_{0.2}Pt_{0.02}O_{2-\delta}$ appears at 74.4 and 77.6 eV which is due to Pt^{4+} oxidation state (Fig. 13a) [35]. Deconvolution of the Pt (4f) peaks reveals that Pt is present only in +4 oxidation state in the as-prepared sample. XPS of the reduced catalyst has Pt (4f) level shifted towards lower binding energy and the peaks are also very broad (Fig. 13b). Peaks were resolved into $4f_{7/2}$ and $4f_{5/2}$ states of Pt^{4+}, Pt^{2+} and Pt^0. Accordingly, the resolved Pt ($4f_{7/2,\ 5/2}$) peaks at

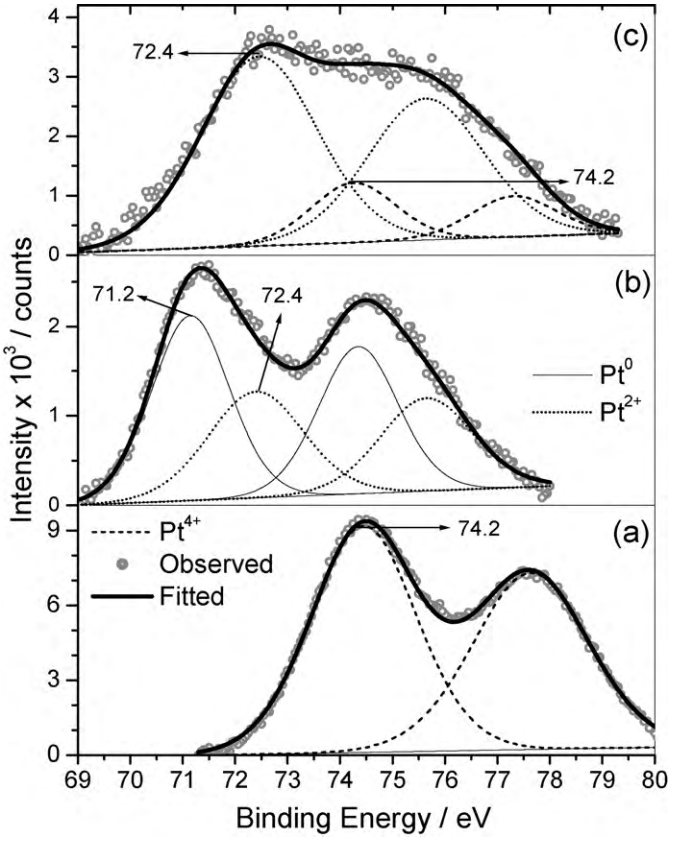

Fig. 13. Pt(4f) core level spectra of (a) as-prepared catalyst, (b) reduced catalyst after start-up/shut-down cycles, and (c) after re-oxidation of the reduced catalyst in air at 550 °C.

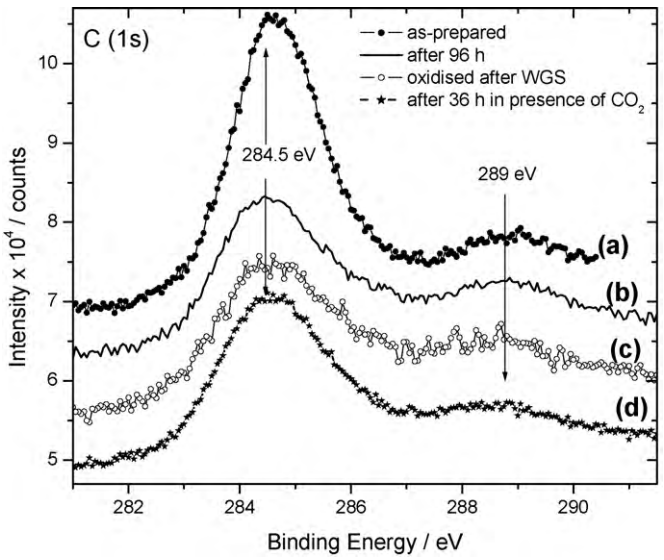

Fig. 14. C(1s) core level spectra of (a) as-prepared catalyst, (b) reduced catalyst after start-up/shut-down cycles, (c) after re-oxidation of the reduced catalyst in air at 550 °C, and (d) spent catalyst after 36 h WGS reaction in presence of CO_2 in the feed gas.

71.2 and 74.3 eV is due Pt^0, and peaks at 72.4 and 75.7 eV represents Pt^{2+} states, and 40% Pt is present in +2 oxidation state. Oxidation of the reduced catalyst shifts the Pt (4f) peaks towards higher binding energy side and are broad suggesting the presence of multiple oxidation states (Fig. 13c). Resolution of the peaks shows that 83% of Pt is present in +2 oxidation state and 17% Pt exist in +4 oxidation state; all metallic-Pt present in the reduced catalyst is, therefore, oxidized. Thus, Ce^{4+}/Ce^{3+}, Sn^{4+}/Sn^{2+} and $Pt^0/Pt^{2+}/Pt^{4+}$ are the active redox couples that participate in the WGS reaction. The color of the reduced catalyst changes from brown color of as-prepared sample to black, indicating the reduction of Sn^{4+} to Sn^{2+} and Pt^{4+} to Pt^{2+}/Pt^0 states.

An estimation of relative concentration of Ce, Sn and Pt of as-prepared, reduced and re-oxidized catalyst were carried out from the intensities of main core level peaks [36]:

$$\text{Concentration, } C_M = \frac{I_M/(\lambda_M \sigma_M D_M)}{\sum(I_M/(\lambda_M \sigma_M D_M))} \quad (3)$$

where I_M is the integrated intensity of the core levels (M = Ce 3d, Sn 3d and Pt 4f), λ_M is the mean escape depths of the respective photoelectrons, σ_M is the photoionization cross section, and D_M is the geometric factor. The photoionization cross section values were taken from Scofield [37], and mean escape depths were taken from Penn [38]. The geometric factor was taken as 1, since the maximum intensity in this spectrometer is obtained at 90°. Accordingly, the relative surface concentration of Ce:Sn:Pt obtained for all three samples were found to be same at 0.79:0.19:0.02 which is close to our experimental ratio.

To check for deactivation of the catalyst due to formation of carbonates or coke over the catalyst surface, C(1s) region of the as-prepared sample and after WGS reaction were recorded. The graphitic carbon peak at 284.5 eV is seen for all the samples. The as-prepared catalyst shows a small peak at 289 eV indicating the presence of surface carbonate (Fig. 14a). XPS of the reduced catalyst after 96 h of start-up/shut-down cycles in absence of excess CO_2 does not show any significant growth in intensity of surface carbonate peak (Fig. 14b). The reduced catalyst was then heated in air at 550 °C for 3 h to decompose any surface carbonates if formed. XPS was then recorded to check for any difference in C(1s) spectra with respect to as-prepared and reduced catalyst. Heated sample does not show any decrease in intensity of the peak at 289 eV (Fig. 14c) implying that no surface carbonate formation took place on the surface of the catalyst after 96 h of reaction. The XPS of the spent catalyst after WGS reaction with excess CO_2 in the feed gas was also examined for carbonate formation (Fig. 14d). C(1s) peak of the spent catalyst does not show any increment in intensity at 289 eV implying that no carbonate formation took place even in presence of excess CO_2. This result indicates that $Ce_{0.78}Sn_{0.2}Pt_{0.02}O_{2-\delta}$ catalyst is resistant to formation of carbonate on the surface due to CO and CO_2 generated in the WGS reaction. This is attributed to reluctance of Sn ion to form any carbonate complex.

3.5. CO oxidation

Since $Ce_{0.78}Sn_{0.2}Pt_{0.02}O_{2-\delta}$ has high activity for WGS reaction with zero deactivating properties, the catalyst was tested for $CO + O_2$ reaction in presence and absence of excess H_2. Fig. 15a shows conversion profiles of 2 and 5 vol% CO in presence stoichiometric O_2 (1 and 2.5 vol% respectively) with N_2 balance at a flow rate of 100 cm^3 min^{-1} over 300 mg of the catalyst. For 2 vol% concentration 100% conversion to CO_2 is observed at 25 °C, and for 5 vol% complete conversion occurs at 35 °C. As high as 5 vol% CO is completely converted to CO_2 at room temperature in presence of stoichiometric oxygen. Because of the availability of activated lattice oxygen in the present catalyst room temperature conversion of CO to CO_2 becomes feasible [39–41].

In absence of feed oxygen, CO oxidation occurs utilizing the activated lattice oxygen. CO oxidation by extracting the available lattice oxygen was carried out with 2 vol% CO balance with nitrogen. The inset of Fig. 15a shows CO oxidation profile with temperature.

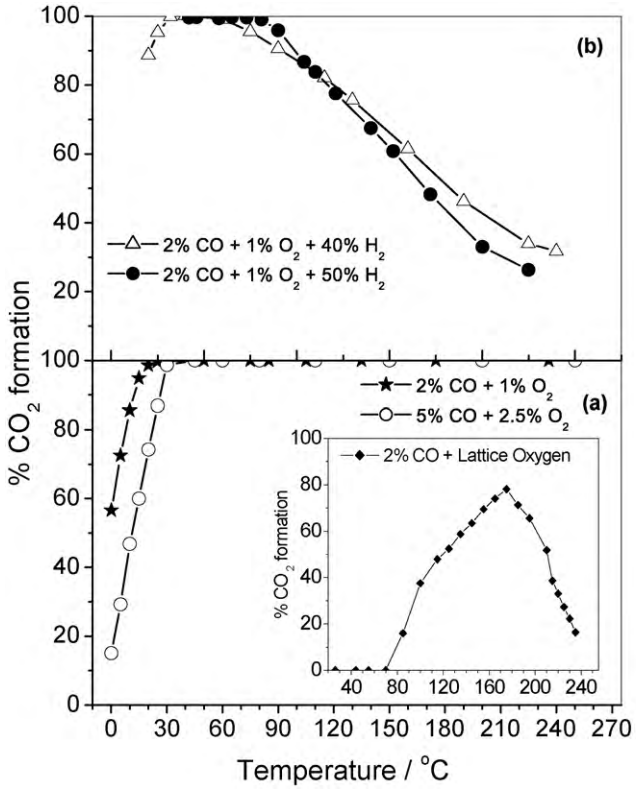

Fig. 15. (a) CO oxidation profiles for different concentrations in presence of stoichiometric O_2. The inset shows CO oxidation (2 vol%) in absence of feed oxygen. (b) PROX of CO in presence of 40 and 50 vol% H_2.

CO_2 formation starts from 70 °C, and 80% conversion is achieved at 180 °C.

3.6. PROX

The aim of the preferential oxidation (PROX) reaction is to selectively oxidize CO, reducing its concentration to <10 ppm for proper operation of fuel cells without consuming the excess hydrogen in the feed gas. Fig. 15b shows PROX reaction of CO in presence of 40 and 50 vol% of hydrogen in the feed gas. 100% CO oxidation occurs at room temperature and above 55 °C conversion rate decreases with increasing temperature. Also with increasing hydrogen concentration (from 40 to 50 vol%) the decrease in the rate of CO conversion increases with temperature. Methane formation did not appear in our experimental conditions due to high selectivity of the catalyst for CO to CO_2 conversion in presence of excess hydrogen. For $Ce_{0.98}Pt_{0.02}O_{2-\delta}$ catalyst 500 ppm of CH_4 is reported to form at 350 °C [22]; therefore by modifying the catalyst by Sn substitution methane formation is completely suppressed in the present catalyst. So the WGS catalyst $Ce_{0.78}Sn_{0.2}Pt_{0.02}O_{2-\delta}$ is also a promising catalyst for PROX at room temperature.

We have observed over 99.5% CO conversion to H_2 in WGS reaction over the catalyst at ~300 °C. CO to CO_2 conversion in presence of stoichiometric O_2 occurs at room temperature and in absence of oxygen CO_2 formation occurs by utilizing lattice oxygen in the temperature range of 70–180 °C. By modifying the catalyst by Sn substitution the OSC of the catalyst is greatly enhanced and amphoteric nature of Sn ensures that the catalyst is resistant to carbonate formation. Oxide ion vacancies created due to CO oxidation provides site for H_2O dissociation leading to generation of H_2 and regeneration of the oxide surface. Therefore oxide vacancies and hence the OSC of the catalyst seems to enhance the rate of H_2 generation by providing additional site for H_2O dissociation.

4. Conclusion

(a) $Ce_{0.78}Sn_{0.2}Pt_{0.02}O_{2-\delta}$ catalyst has been synthesized first time following solution combustion method. $Ce_{0.78}Sn_{0.2}Pt_{0.02}O_{2-\delta}$ crystallizes in fluorite structure with lattice parameter $a = 5.39$ Å.

(b) H_2-TPR measurement of the catalyst shows very high OSC corresponding to 3500 μmol g^{-1} at 80 °C. This implies that 0.63 mol of O can be reversibly extracted from the lattice per mole of the catalyst under reducing atmosphere of CO or H_2.

(c) $Ce_{0.78}Sn_{0.2}Pt_{0.02}O_{2-\delta}$ is an excellent catalyst for WGS with >99.5% conversion for 2 vol% of CO at 275 °C. No deactivation of the catalyst due to carbonate formation or sintering of noble metal ion was observed under stringent start-up/shut-down cycles for 96 h. WGS reaction in presence of hydrogen leads to formation of CO_2 and H_2 only and side products such as methane, methanol, formaldehyde etc. were not observed up to reaction temperature of 500 °C.

(d) CO oxidation in presence of stoichiometric oxygen shows complete conversion at room temperature. PROX in presence of excess hydrogen shows high selectivity and activity of the catalyst for CO oxidation at room temperature. This property of the catalyst finds application in processing of reformer feed to fuels cells where trace amount (<10 ppm) of CO has detrimental effect on Pt-anode of the fuel cell.

Acknowledgements

We thank Indian Council of Agricultural Research (ICAR) and Department of Science and Technology (DST), Government of India for financial support.

References

[1] P.T. Anastas, J.C. Warner (Eds.), Green Chemistry: Frontiers in Benign Chemical Synthesis and Processes, Oxford University Press, Oxford, 1998.
[2] P.T. Anastas, M.M. Kirchhoff, Acc. Chem. Res. 35 (2002) 686–694.
[3] J. Heiko, Angew. Chem. Int. Ed. 43 (2004) 1912–1914.
[4] S. Vasileiadis, Z. Ziaka-Vasileiadou, Chem. Eng. Sci. 59 (2004) 4853–4859.
[5] H.-F. Oetjen, V.M. Schmidt, U. Stimming, F. Trila, J. Electrochem. Soc. 143 (1996) 3838–3842.
[6] E. Xue, M. O'Keeffe, J.R.H. Ross, Catal. Today 30 (1996) 107–118.
[7] S. Hilaire, X. Wang, T. Luo, R.J. Gorte, J. Wagner, Appl. Catal. A 258 (2004) 271.
[8] T. Bunluesin, R.J. Gorte, G.W. Graham, Appl. Catal. B 15 (1998) 107–114.
[9] Q. Fu, H. Saltsburg, M. Flytzani-Stephanopoulos, Science 301 (2003) 935.
[10] E. Fox, A. Lee, K. Wilson, C. Song, Top. Catal. 49 (2008) 89–96.
[11] C. Yeung, S. Tsang, Catal. Lett. 128 (2009) 349–355.
[12] N. Schumacher, A. Boisen, S. Dahl, A.A. Gokhale, S. Kandoi, L.C. Grabow, J.A. Dumesic, M. Mavrikakis, I. Chorkendorff, J. Catal. 229 (2005) 265–275.
[13] J.C. Serrano-Ruiz, G.W. Huber, M.A. Sánchez-Castillo, J.A. Dumesic, F. Rodríguez-Reinoso, A. Sepúlveda-Escribano, J. Catal. 241 (2006) 378–388.
[14] R. Si, M. Flytzani-Stephanopoulos, Angew. Chem. Int. Ed. 47 (2008) 2884–2887.
[15] C.T. Campbell, C.H.F. Peden, Science 309 (2005) 713–714.
[16] J.L.C. Fajin, F. Illas, J.R.B. Gomes, J. Chem. Phys. 130 (2009) 224702–224708.
[17] X. Liu, W. Ruettinger, X. Xu, R. Farrauto, Appl. Catal. B 56 (2005) 69.
[18] J.M. Zalc, V. Sokolovskii, D.G. Löffler, J. Catal. 206 (2002) 169–171.
[19] M.S. Hegde, G. Madras, K.C. Patil, Acc. Chem. Res. 42 (2009) 704–712.
[20] U. Lassi, Deactivation Correlations of Pd/Rh Three-way Catalysts Designed for Euro IV Emission Limits: Effect of Ageing Atmosphere, Temperature and Time, Dissertation Department of Process and Environmental Engineering, University Of Oulu, 2003, p. 35.
[21] Q. Fu, W. Deng, H. Saltsburg, M. Flytzani-Stephanopoulos, Appl. Catal. B 56 (2005) 57–68.
[22] S. Sharma, P.A. Deshpande, M.S. Hegde, G. Madras, Ind. Eng. Chem. Res. 48 (2009) 6535–6543.
[23] G. Jacobs, E. Chenu, P.M. Patterson, L. Williams, D. Sparks, G. Thomas, B.H. Davis, Appl. Catal. A 258 (2004) 203–214.
[24] L. Dorazio, W. Ruettinger, M.J. Castaldi, R. Farrauto, Top. Catal. 51 (2008) 68–75.
[25] A. Goguet, R. Burch, Y. Chen, C. Hardacre, P. Hu, R.W. Joyner, F.C. Meunier, B.S. Mun, D. Thompsett, D. Tibiletti, J. Phys. Chem. C 111 (2007) 16927–16933.
[26] A.M. Duarte de Farias, D. Nguyen-Thanh, M.A. Fraga, Appl. Catal. B 93 (2010) 250–258.
[27] A.M. Duarte de Farias, P. Bargiela, M.d.G.C. Rocha, M.A. Fraga, J. Catal. 260 (2008) 93–102.

[28] J. Rodriguez-Carvajal, Multi-pattern Rietveld Refinement program Fullprof. 2k, version 3.30 June 2005-LLB.
[29] A.A. Phatak, N. Koryabkina, S. Rai, J.L. Ratts, W. Ruettinger, R.J. Farrauto, G.E. Blau, W.N. Delgass, F.H. Ribeiro, Catal. Today 123 (2007) 224–234.
[30] H.C. Yao, Y.F.Y. Yao, J. Catal. 86 (1984) 254–265.
[31] P. Bera, A. Gayen, M.S. Hegde, N.P. Lalla, L. Spadaro, F. Frusteri, F. Arena, J. Phys. Chem. B 107 (2003) 6122–6130.
[32] T. Baidya, A. Gupta, P.A. Deshpandey, G. Madras, M.S. Hegde, J. Phys. Chem. C 113 (2009) 4059–4068.
[33] A. Kotani, H. Ogasawara, J. Electron. Spectrosc. Relat. Phenom. 60 (1992) 257–299.
[34] D. Briggs, M.P. Seah, Practical Surface Analysis, John Wiley & Sons Ltd., New York, 1983.
[35] T. Baidya, A. Gayen, M.S. Hegde, N. Ravishankar, L. Dupont, J. Phys. Chem. B 110 (2006) 5262–5272.
[36] C.J. Powell, P.E. Larson, Appl. Surf. Sci. 1 (1978) 186–201.
[37] J.H. Scofield, J. Electron. Spectrosc. Relat. Phenom. 8 (1976) 129–137.
[38] D.R. Penn, J. Electron Spectrosc. Relat. Phenom. 9 (1976) 29–40.
[39] M. Nolan, V.S. Verdugo, H. Metiu, Surf. Sci. 602 (2008) 2734–2742.
[40] R.G.S. Pala, W. Tang, M.M. Sushchikh, J.-N. Park, A.J. Forman, G. Wu, A. Kleiman-Shwarsctein, J. Zhang, E.W. McFarland, H. Metiu, J. Catal. 266 (2009) 50–58.
[41] V. Shapovalov, H. Metiu, J. Catal. 245 (2007) 205–214.